

Lloyd's mirror interference lithography with EUV radiation from a high-harmonic source

This content has been downloaded from IOPscience. Please scroll down to see the full text.

2016 Appl. Phys. Express 9 076701

(<http://iopscience.iop.org/1882-0786/9/7/076701>)

View [the table of contents for this issue](#), or go to the [journal homepage](#) for more

Download details:

IP Address: 152.78.130.228

This content was downloaded on 12/08/2016 at 14:18

Please note that [terms and conditions apply](#).

Lloyd's mirror interference lithography with EUV radiation from a high-harmonic source

Hyun-su Kim^{1,2,4*}, Peter Baksh¹, Michal Odstrcil^{1,2}, Magdalena Miszczak¹, Jeremy G. Frey³, Larissa Juschkina^{2,4}, and William S. Brocklesby¹

¹Optoelectronics Research Centre, University of Southampton, Southampton SO17 1BJ, U.K.

²Chair for the Experimental Physics of Extreme Ultraviolet, RWTH Aachen University, JARA FIT, 52074 Aachen, Germany

³School of Chemistry, University of Southampton, Southampton SO17 1BJ, U.K.

⁴Peter Grünberg Institut (PGI-9), Forschungszentrum Jülich GmbH, JARA-FIT, 52425 Jülich, Germany

Received April 28, 2016; accepted May 25, 2016; published online June 9, 2016

We demonstrate interference lithography using a high-harmonic source. Extreme ultraviolet (EUV) radiation is produced by high-harmonic generation with 800 nm light from a femtosecond Ti:sapphire laser (40 fs pulses, 1 kHz, 2 W average power) in argon gas. Interference patterns created using Lloyd's mirror setup and monochromatized radiation at the 27th harmonic (29 nm) are recorded using a ZEP-520A photoresist, producing features with <200 nm pitch. The effect of the use of femtosecond pulsed EUV radiation on the recorded pattern is investigated. The capability of the high-harmonic source for high-resolution patterning is discussed. © 2016 The Japan Society of Applied Physics

Extreme ultraviolet (EUV) interference lithography (IL) is a powerful method of fabricating high-resolution patterns over a large area without a complex imaging system. The main requirement for EUV-IL is high-intensity coherent plane wave illumination in order to deliver a sufficient radiation dose to the photoresist plane. A particular issue is the availability of appropriate optical components such as beam splitters and reflective or spectrally filtering mirrors for the particular optical wavelength used. Those components can be obtained easily in the case of using radiation in the spectral range over deep ultraviolet, ultraviolet, and IR lasers where refractive optical elements are available.^{1–3)}

When using EUV or soft X-ray radiation, different strategies to split and recombine parallel beams have been demonstrated such as those using reflective beam splitters^{4–7)} or multiple diffraction gratings.^{8,9)} These demonstrations were performed with both a synchrotron radiation source and a plasma-based EUV laser. In the demonstration performed using synchrotron radiation, the monochromatized and spatially filtered light at a wavelength of 13.5 nm from an undulator provided the necessary temporal and spatial coherences with sufficient intensity flux.⁴⁾ The plasma-based EUV laser is also a suitable radiation source for IL as it was demonstrated using a compact Ne-like Ar capillary discharge laser at a wavelength of 46.9 nm producing an EUV radiation of around 0.2 mJ with a maximum repetition rate of 10 Hz.⁶⁾

Interference lithography has also been performed in the UV and IR spectral ranges with femtosecond pulsed lasers.^{3,10,11)} The second harmonic of femtosecond pulses (380 nm, 80 fs, 82 MHz) was split by a diffractive beam splitter and overlapped with two lenses.¹⁰⁾ A femtosecond laser pulse (800 nm, 90 fs) was used for lithographical laser ablation to fabricate a homogeneous metal nanograting.^{3,11)} The EUV-IL demonstrations using a synchrotron radiation source and a plasma-based EUV laser have used radiation with a pulse duration of around 1–2 ns. The effect of high-density ionization using ultrashort EUV pulses generated by a free electron laser (FEL) on the sensitivity of a nonchemi-

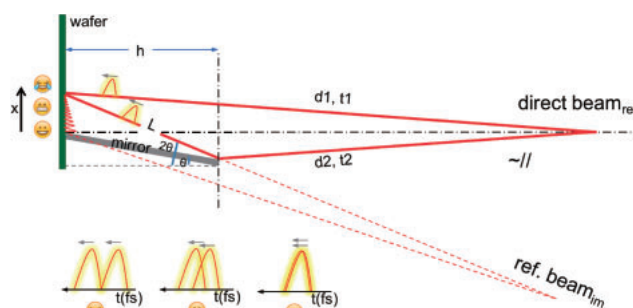


Fig. 1. Schematic of the Lloyd mirror IL with a focusing beam: reflected and direct beams having different optical paths (d) and arrival times (t) are illustrated. The angle of the mirror is θ from normal. The visibility of fringes decreases away from the edge owing to the optical path difference between two short pulses.

cally amplified resist was investigated.¹²⁾ It was shown that multiple reactions with ultrahigh-brightness pulses provided by EUV-FEL radiation change the sensitivity of the resist.

High-harmonic generation (HHG) provides coherent radiation in a wide EUV spectral range (10–40 nm) with emission peaks at the odd harmonics of the driving laser field, ω . The degree of temporal coherence of each individual peak is on the order of $\Delta\lambda/\lambda \sim 10^{-3}$. The spatial coherence length depends on the HHG phase-matching process in the gas-cell-based high-harmonic source. The high spatial coherence and low divergence of the HHG beam were already presented.^{13,14)}

In this work, we demonstrate Lloyd's mirror IL with EUV radiation generated by a HHG source. The demonstration was performed with a monochromatized radiation centered at a wavelength of around 29 nm, and the small angle in Lloyd's mirror setup allows us to achieve fringes with sub-200 nm pitch. We analyze the expected optical properties of the interference fringes in the photoresist.

The interference fringes are formed owing to constructive and destructive interferences between the split beams of the reflected wave and the direct wave in Lloyd's mirror arrangement (Fig. 1). The period (pitch) of the interference fringe, which is determined by the angle between two beams, is given by

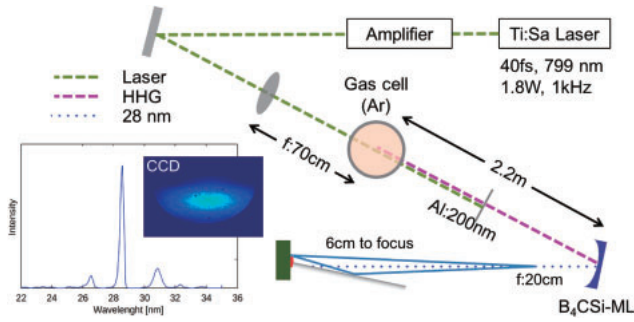


Fig. 2. Schematic of HHG and Lloyd’s mirror IL: The laser is s-polarized. The inset image is the spectrum of the EUV after the ML mirror. The CCD image of the beam is stretched by the spherical mirror.

$$\text{pitch} = \frac{\lambda}{2 \sin \theta}, \quad (1)$$

where θ is the half-angle between two interfering waves. The number of pitches (N) in the interference field is limited by the temporal coherence of the incident beam given by

$$N \leq \lambda/\Delta\lambda, \quad (2)$$

owing to the phase delay of the reflected wave interacting with the direct wave. In this experiment, $\lambda/\Delta\lambda \approx 250$ was estimated.

Figure 1 illustrates the Lloyd’s mirror IL setup of the experiment. The divergence of the EUV beam after the gas cell is around 1–2 mrad, and after the spherical mirror, it is around 5–15 mrad in Fig. 2. In the analysis, we assume that the incidence angle of the direct beam is approximated to a normal angle, and the angle of the reflected beam is approximated to be twice the mirror’s angle (2θ). In Lloyd’s mirror system, a reflective mirror splits part of the incident beam and redirects the reflected part to generate a second beam. During this separation, an optical path difference (OPD) between the two beams occurs. Using fs-pulsed radiation, the OPD has to be controlled in the range of only a few micrometers. The fringe profile visibility decreases away from the edge (the line shared by the photoresist and mirror planes) owing to the increase in OPD.

The OPD yields time delay for the reflected beam arriving at the target plane. It is approximately “ $L - h$ ”, as illustrated in Fig. 1, and increases with the angle (θ). In the photoresist plane, the delay increases proportionally with the distance (x in Fig. 1) from the edge. The field length of the fringe along the x -direction is estimated to be $\text{OPD} \times [\tan(2\theta) - \tan\theta]/[1/\cos(2\theta) - 1]$ from a geometrical approximation. The time difference between two pulses is OPD/c (c : speed of light in vacuum), which must not exceed the pulse duration, “ $L - h = \text{OPD} < \text{pulse duration} \times c$ ”. The temporal overlap of the two pulses, which determines the interference term, decreases with the OPD. Also, the interference region depends on the angle θ and pulse duration. A rapid reduction in visibility is expected when $\theta > 15^\circ$.

The intensity profile of interference fringes can be described as follows:

$$I = I_1 + I_2 + 2(I_1 I_2)^{1/2} \text{Re} \gamma_{12}(\tau), \quad (3)$$

where I_1 and I_2 are the intensities of the direct and reflected beams, respectively. $\gamma_{12}(\tau)$ is the interference term, where τ

is the time difference of two optical paths, which is called the degree of partial coherence.^{15,16)}

The visibility of interference fringes is given by

$$V = \frac{I_{\max} - I_{\min}}{I_{\max} + I_{\min}} = \frac{2\sqrt{I_1 I_2} |\gamma_{12}|}{I_1 + I_2}. \quad (4)$$

In the lithographic performance, fringe visibility depends on the photoresist response. The depth of radiation that induced grooves depends on the fluence (mJ/cm^2).

In EUV radiation, the interference region (x) is also affected by the mirror’s reflectivity. The maximum angle is limited to around 20° with a thick Si mirror for radiation with a wavelength of 29 nm. We use a Si mirror at $\theta \approx 3\text{--}4^\circ$, providing reflectivity of around 95% for the EUV wavelengths used in this demonstration.

Our experimental setup is illustrated in Fig. 2. We use a HHG system based on a Ti:sapphire laser (800 nm, 40 fs) amplified by a regenerative chirped pulsed amplifier (CPA). The laser beam ($10^{14} \text{ W}/\text{cm}^2$ at the gas cell position, 1.8 mJ/pulse, 1 kHz repetition rate) is focused into a 3-mm-long gas cell filled with argon gas at 60 mbar. The strong E-field has a pulse duration of around 40 fs. A single Al foil (200 nm thickness) is used to block the fundamental laser and transmit the EUV radiation (approximately 30% transmission). Then, in order to suppress unwanted spectral components, the beam is spectrally filtered by a curved $\text{B}_4\text{C}/\text{Si}$ multilayer (ML) mirror, which reflects and focuses the main wavelength at $\sim 29 \text{ nm}$ (27th harmonic, $\Delta\lambda/\lambda \sim 4 \times 10^{-3}$) and ± 1 harmonics from the main wavelength with very low intensity. The spectrum after the ML mirror is shown in the inset image in Fig. 2. The Gaussian-shaped illumination profile measured using an EUV-sensitive CCD camera (Andor DX-434, 1024×1024 pixels) is shown in the inset CCD image in Fig. 2. The estimated photon flux is $\sim 1.86 \times 10^9$ photons/s in the whole area of the spot.¹⁹⁾

Before performing the IL, we conducted exposure tests for a photoresist sample. We used a positive-tone photoresist (dilution ratio: ZEP-520A : anisole = 1 : 3). The photoresist was spin-coated (5000 rpm, 1 min) on a silicon wafer for the target thickness of $\sim 40\text{--}60 \text{ nm}$ and baked for 2 min at 180°C on a hotplate. In the setup (vacuum chamber), the photoresist-coated wafer was mounted perpendicularly to the beam. The exposure time was varied from 0.5 to 15 s at several positions between $\pm 5 \text{ mm}$ from the EUV focus in order to record the cross-sectional profile of the beam. After the exposure, the wafer was developed with ZED N50 for 90 s and rinsed with 2-propanol for 30 s. The obtained result was investigated with an optical microscope (Nikon Eclipse-L200) to measure the intensity profile of the beam. It was analyzed in terms of the dependence of the removed resist thickness on the radiant fluence (exposure dose), which is related to the lithographic sensitivity of the photoresist with the EUV radiation. The thickness dependence of the removed photoresist (depth from the surface) on fluence is plotted in Fig. 3.

ZEP-520A is a positive-tone photoresist, which is a modern alternative to poly(methyl methacrylate) (PMMA), based on the copolymer compound (Zeon). The molecular mechanisms of ZEP-520A are not entirely understood yet.¹⁷⁾

The photoresist processing is separated into exposure and development. Typical positive photoresists are composed of a photoactive compound, a base resin, and a suitable

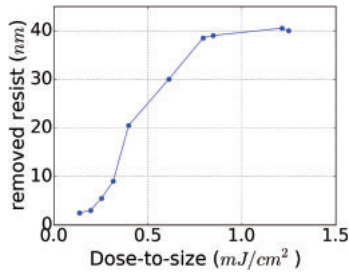


Fig. 3. Depth of removed photoresist depending on the exposure dose.

organic solvent system. The base resin, which is soluble with developers, is protected by the photoactive compound (inhibitor). The radiant energy delinks the inhibitor from the resin and results in an increased photoresist dissolution rate. Thus, exposure wavelength (photon energy) is an important parameter of resist sensitivity.¹⁸⁾

There are two issues with the use of short-pulse radiation in Lloyd's mirror IL. The first one is the arrangement for interference, as discussed. The other issue is the interaction between the resist and the short-pulse radiation. The EUV pulse length from HHG sources is on the order of femtosecond duration. This is very different from the plasma-based EUV radiation, which typically yields nanosecond pulses and is a quasi-CW (continuum wave) on the timescale of the exposure process.

The probability of delink decreases with increasing flux density at an identical exposure dose. The single photon breaks the cross-link within a particular radical distance. The spatiotemporal overlap of photons reduces the effectiveness, while the high radical concentration enhances local delinks. The use of short pulse (high-density flux) enhances competing effects resulting in different exposure sensitivities.¹²⁾ It might be interesting to compare our result with that from plasma-based sources or synchrotron radiations in the future.

The Lloyd's mirror IL was performed with the photoresist produced as described previously. The ZEP-520A-coated wafer was mounted on a nanoprecision piezo stage (SmarAct-SLC-1730) at an angle normal to the beam path. The photoresist plane was located at the z -position around $z = +6$ mm (toward photoresist) from the focal plane of the ML, which is an optimized location for sufficient exposure conditions, given the field size of the beam ($\sim 200 \times 50 \mu\text{m}^2$) and the exposure time of ~ 9 s. After the exposure, the photoresist was developed with ZED N50 for 90 s and rinsed with 2-propanol for 30 s. The resulting patterns were analyzed by atomic force microscopy (AFM; Bruker).

The resulting AFM image in Fig. 4(a) shows a pattern with a period of 198 nm, corresponding to a mirror angle of 4.2° . Figure 4(b) is the cross section of (a). The groove depth (Δd) along the x -axis is measured as plotted in Fig. 4(c) and clearly drops as a function of distance from the mirror edge. There are several reasons for the drop. Firstly, the transverse intensity profile of the Gaussian beam drops away from the edge, where the right half is flipped over the mirror with a reflection of $\sim 95\%$ in Lloyd's mirror scheme. Secondly, the time delay between the reflected beam and the direct beam increases away from the edge. As the interfering time decreases, the degree of mutual coherence decreases resulting in the drop of fringe visibility.

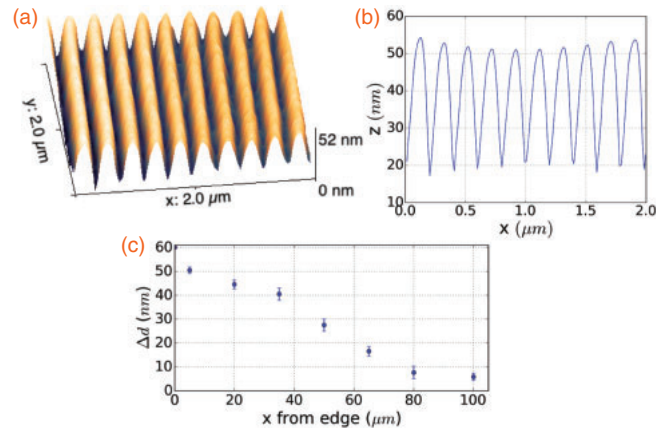


Fig. 4. (a) AFM image of the patterned photoresist, (b) thickness profile showing a half-period of 99 nm, and (c) groove depth along x -axis.

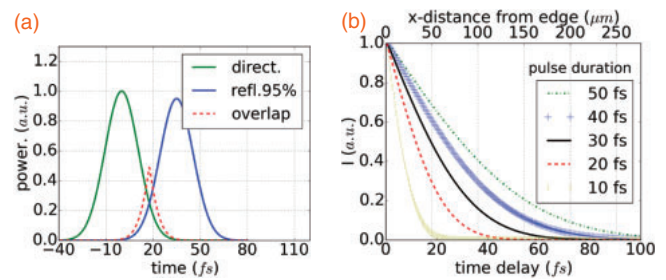


Fig. 5. (a) Pulses of the direct and reflected beams with the time delay. The pulses partially overlap depending on both the OPD and the pulse duration. (b) Integration of the overlap as a function of the time delay for several pulse durations.

In the photoresist, the depth (d) after the lithographic process can be derived as $d = [1 - \exp(-\alpha t)]D$, where α is the lithographic factor related to photoresist sensitivity, t is the exposure time, and D is the initial thickness of the photoresist. Then, the groove depth can be given by

$$\Delta d = \{1 - \exp[-\alpha(I_{\max} - I_{\min})t]\}D. \quad (5)$$

Applying $(I_{\max} - I_{\min}) = 2(I_1 + I_2)V$ to Eq. (5), we obtain the following relationship between Δd and V :

$$\Delta d/D = 1 - \exp[-2\alpha(I_1 + I_2)Vt]. \quad (6)$$

Thus, the fringe visibility V can be written as

$$V = -\frac{\ln(1 - \Delta d/D)}{2\alpha(I_1 + I_2)t}. \quad (7)$$

In principle, the intensity distribution of interference fringes is given by the time-averaged sum of two electric fields. We now have to consider the time integral over the pulse duration. For nano- or picosecond pulses, the change in time integral is negligible along the x -axis owing to the long pulse duration. However, for the pulses below 100 fs, the time integration term drops quickly away from the mirror edge. In the interference term of the fringe in Eq. (3), I_2 is delayed. Thus, I_2 can be rewritten as $I_2' = I_2 \times O_{(x)}$, where $O_{(x)}$ is an overlap factor with a normalized value shown in Fig. 5(b), which depends on the pulse duration.

A typical Gaussian shape pulse is plotted in Fig. 5(a), where the pulse length is assumed to be the full-width at half maximum (FWHM) of the pulse. Figure 5(a) shows direct and

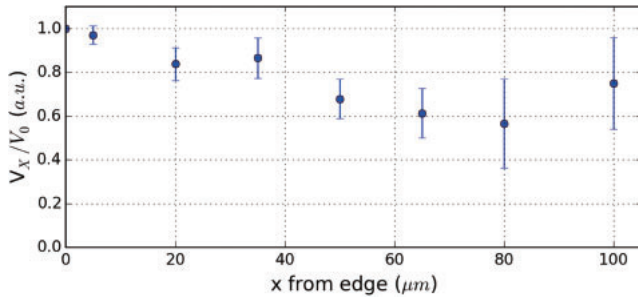


Fig. 6. Visibility over the edge region with the assumption that the pulse duration of the EUV light is 30 fs.

reflected pulses with some time delay. The partial overlap of the pulses in time depends on both the OPD and the pulse duration. The overlap decreases as the OPD increases or as the pulse duration decreases, as plotted in Fig. 5(b). Pulse durations from 10 to 50 fs are investigated. The overlapping area drops more quickly as the pulse duration decreases.

The visibility for a short-pulse radiation interference pattern can be written as $V(I_1, I_2)$. In order to eliminate the unknown factor α , we plot the visibility as

$$V_{(x)}/V_0 = -\ln(1 - \Delta d_{(x)}/D) \times I_0/I_{(x)}, \quad (8)$$

where $V_0 = V_{(x=0)}$, $I_0 = I_{1,(x=0)} + I'_{2,(x=0)}$, and $I_{(x)} = I_{1,(x)} + I'_{2,(x)}$. Figure 6 shows the results obtained using Eq. (8) with different distances from the edge. The visibility is >0.55 over the investigated area. The visibility is not significantly reduced in the investigated x -range.

In conclusion, we have demonstrated Lloyd's mirror interference lithography using radiation from a HHG system. The monochromatized EUV radiation generated by the HHG source enables us to perform laboratory lithographic fabrication for high-density periodic structures. The exposure sensitivity of the ZEP-520A photoresist is obtained for the radiation used. The fringe visibility over the field is measured and corresponds well to a model that includes the effects of the Gaussian beam profile, the optical path difference, and the pulse duration. The reflectivity of the mirror, the degree of mutual coherence, and the overlap of two pulses affect the visibility. In the future, patterning with sub-60 nm pitch (30 nm half-pitch) is expected to be possible using

Lloyd's mirror angles up to 15° with the radiation used in this work.

Acknowledgments This work was supported by the EPSRC Basic Technology program (GR/R87307/01). H.K., M.O., and M.M. acknowledge financial support from the EU FP7 Erasmus Mundus Joint Doctorate Programme EXTATIC under framework partnership agreement FPA-2012-0033. P.B. acknowledges the EPSRC studentship (EP/K503150/1, EP/P505739/1, EP/J500537/1). L.J. acknowledges financial support from the Helmholtz Association for a Helmholtz Professorship as a part of the Initiative and Networking Fund. The data for this work is accessible through the University of Southampton Institutional Research Repository.

- 1) S. Brueck, *Proc. IEEE* **93**, 1704 (2005).
- 2) I. Wathuthanthri, Y. Liu, K. Du, W. Xu, and C. Choi, *Adv. Funct. Mater.* **23**, 608 (2013).
- 3) K. Miyazaki, G. Miyaji, and T. Inoue, *Appl. Phys. Lett.* **107**, 071103 (2015).
- 4) H. Solak, D. He, W. Li, S. Singh-Gasson, F. Cerrina, B. Sohn, X. Yang, and P. Nealey, *Appl. Phys. Lett.* **75**, 2328 (1999).
- 5) A. Ritucci, A. Reale, P. Zuppella, L. Reale, P. Tucceri, G. Tomassetti, P. Bettotti, and L. Pavesi, *J. Appl. Phys.* **102**, 034313 (2007).
- 6) P. Wachulak, P. Wachulak, M. Capeluto, M. Marconi, C. Menoni, and J. Rocca, *Opt. Express* **15**, 3465 (2007).
- 7) P. Zuppella, D. Luciani, P. Tucceri, P. Marco, A. Gaudieri, J. Kaiser, L. Ottaviano, S. Santucci, and A. Reale, *Nanotechnology* **20**, 115303 (2009).
- 8) H. Solak, *J. Phys. D* **39**, R171 (2006).
- 9) N. Mojarad, D. Fan, J. Gobrecht, and Y. Ekinci, *Opt. Lett.* **39**, 2286 (2014).
- 10) T. Kondo, S. Matsuo, S. Juodkazis, and H. Misawa, *Appl. Phys. Lett.* **79**, 725 (2001).
- 11) Y. Nakata, T. Okada, and M. Maeda, *Appl. Phys. A* **79**, 1481 (2004).
- 12) K. Okamoto, T. Kozawa, K. Oikawa, T. Hatsui, M. Nagasono, T. Kameshima, T. Togashi, K. Tono, M. Yabashi, H. Kimura, Y. Senba, H. Ohashi, R. Fujiyoshi, and T. Sumiyoshi, *Appl. Phys. Express* **5**, 096701 (2012).
- 13) J. Zhou, J. Peatross, M. Murnane, H. Kapteyn, and I. Christov, *Phys. Rev. Lett.* **76**, 752 (1996).
- 14) R. A. Bartels, A. Paul, H. Green, H. C. Kapteyn, M. M. Murnane, S. Backus, I. P. Christov, Y. Liu, D. Attwood, and C. Jacobsen, *Science* **297**, 376 (2002).
- 15) B. J. Thompson and E. Wolf, *J. Opt. Soc. Am.* **47**, 895 (1957).
- 16) G. R. Fowles, *Introduction to Modern Optics* (Dover, New York, 1975) 2nd ed.
- 17) K. Koshelev, M. Mohammad, T. Fito, K. Westra, S. Dew, and M. Stepanova, *J. Vac. Sci. Technol. B* **29**, 06F306 (2011).
- 18) F. Dill, W. Hornberger, P. Hauge, and J. Shaw, *IEEE Trans. Electron Devices* **22**, 445 (1975).
- 19) The number of photons per second is determined by $N_{\text{ph/s}} = (S_{\text{CCD}} \cdot \sigma) / [\eta_{\text{QE}} \cdot (E_{\text{ph}}/3.65\text{eV}) \cdot t_{\text{exp}}]$, where S_{CCD} : counted signal on the CCD, σ : CCD sensitivity in electrons per count, η_{QE} : quantum efficiency of the CCD, E_{ph} : photon energy, and t_{exp} : exposure time ($\sigma = 2$, $\eta_{\text{QE}} = 0.3$, $E_{\text{ph}} = 43\text{eV}$, $t_{\text{exp}} = 0.05\text{s}$, $S_{\text{CCD}} = 1.6 \times 10^8$).